Science of the Total Environment 960 (2025) 178283

Contents lists available at ScienceDirect

Science of the Total Environment

journal homepage: www.elsevier.com/locate/scitotenv

Role of factors controlling diurnal variation of cold-season formaldehyde during Satellite Integrated Joint Monitoring of Air Quality 2021 campaign

Lim-Seok Chang [a,*], Soi Ahn [a], Min-Suk Bae [b], Seung-Myung Park [a], Junsu Gil [c], Kwang-Rae Kim [d], Gangwoong Lee [e], Taehyoung Lee [e], Jung-Hun Woo [f], Rokjin Park [f], Hyeong-Ahn Kwon [g], Gyo-Hwang Choo [a], Chang-Keun Song [h,*]

[a] National Institute of Environmental Research, Incheon, Republic of Korea
[b] Department of Environmental Engineering, Mokpo National University, Republic of Korea
[c] Korea University, Seoul, Republic of Korea
[d] Seoul Research Institute of Public Health and Environment, Seoul, Republic of Korea
[e] Hankuk University of Foreign Studies, Gyeonggi, Republic of Korea
[f] Seoul National University, Seoul, Republic of Korea
[g] University of Suwon, Hwaseong-si, Gyeonggi-do, Republic of Korea
[h] Ulsan National Institute of Science and Technology, Ulsan, Republic of Korea

HIGHLIGHTS

- The mixed-layer model showed a bias between the modeled and observed HCHO concentrations in Seoul's PBL.
- FT-PBL VOCs variations caused up to 119.4 % difference in daily HCHO.
- Morning HCHO was driven by primary emissions, daytime HCHO by FT-PBL exchange, and secondary production.
- Primary emissions were as important as secondary production in cold seasons.
- Reducing VOC emissions effectively decreased HCHO and O_3 in Seoul.

GRAPHICAL ABSTRACT

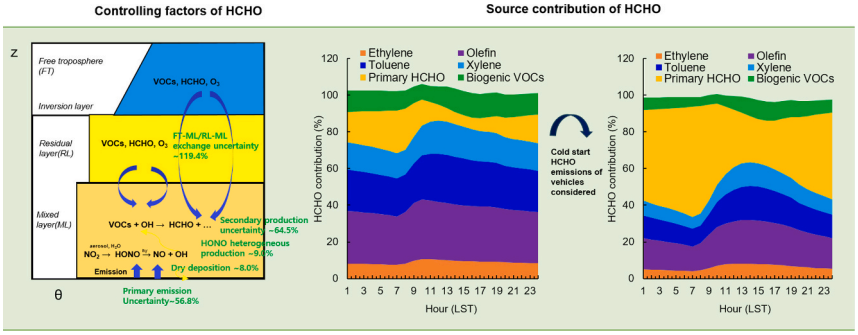

ARTICLE INFO

Editor: Hai Guo

ABSTRACT

Formaldehyde (HCHO), a major carbonyl compound in urban air, poses health risks due to its carcinogenic properties. However, the role of FT-PBL exchange in HCHO and the importance of vertical exchange on diurnal variations in HCHO remain unclear. This study investigated the diurnal variability of HCHO in Seoul's planetary boundary layer (PBL) during cold. We examined the impacts of (1) the exchange between the free troposphere (FT) and PBL, (2) primary emissions and secondary HCHO production, (3) heterogeneous nitrous acid production, and (4) dry deposition. Variations in the relationship of VOC precursors between FT and PBL resulted in up to 119.4 % difference in the daily average HCHO. Uncertainties in VOCs and HCHO emissions led to daily average HCHO variabilities of 64.5 % and 56.8 %, respectively. Morning HCHO was sensitive to primary HCHO emissions, whereas daytime HCHO was sensitive to VOC emissions and FT-PBL exchange. Heterogeneous

* Corresponding authors.
E-mail addresses: lschang@korea.kr (L.-S. Chang), cksong@unist.ac.kr (C.-K. Song).

https://doi.org/10.1016/j.scitotenv.2024.178283
Received 10 October 2024; Received in revised form 4 December 2024; Accepted 22 December 2024
Available online 9 January 2025

production/dry deposition increased/decreased HCHO levels to a much lesser extent (9.0 % and 8.0 %, respectively). The contribution of VOC precursor emissions was superior to that of primary HCHO emissions, and the important species/classes of VOC precursors were ordered as olefins, toluene, xylene, and ethylene. However, when considering the impact of cold climates on primary emissions from vehicles, the proportion increased to a level comparable to that of secondary HCHO production. These findings highlight the need for accurate VOC and HCHO emission data and vertical profiles to understand diurnal HCHO variations and guide strategies to reduce VOC emissions and mitigate HCHO and O_3 in Seoul.

1. Introduction

Formaldehyde (HCHO) is the most abundant carbonyl compound in urban air and poses health risks due to its carcinogenic properties (IARC, 2006). It is ubiquitous and is generated from both natural sources and anthropogenic activities (Vrekoussis et al., 2010), with additional indoor sources, including building materials and consumer products (Gupta et al., 1982). HCHO is integral to photochemical processes and acts as both a source and sink of free radicals. It is photolyzed to form an atomic hydrogen radical, which reacts with oxygen to produce a hydroperoxyl radical (HO_2). HO_2 is subsequently converted to hydroxyl radicals (OH), which are the most crucial oxidizing species in the atmosphere. Additionally, HCHO promotes ozone formation through its oxidizing capacity and participates in in-cloud chemistry, thereby contributing to aerosol production (Dovrou et al., 2022).

Ambient HCHO is governed by various atmospheric processes including NO_x–volatile organic compound (VOC)–O_3–HO_x chemistry, free troposphere (FT)-Planetary Boundary Layer (PBL) exchange, surface emissions, and dry/wet deposition. Earlier studies have attempted to apportion ambient HCHO between primary and secondary sources. Possanzini et al. (2002) demonstrated that the contribution of secondary HCHO production could vary significantly, ranging from below 35 % to 80–90 %, depending on the season. Garcia et al. (2006) attributed a significant amount of HCHO to primary emissions in Mexico City during the spring of 2003 using the CO–CHOCHO tracer pair. This emphasizes the equal importance of primary and secondary HCHO as control strategies. Subsequent studies identified VOC species important for secondary HCHO production in major cities. Wu et al. (2023) quantified the HCHO production rates for 24 VOC species and identified alkenes as key precursors in Shanghai during the summer.

In addition to emissions and chemistry, their interaction with turbulence is another important factor controlling HCHO emissions under diurnally varying PBL conditions. Vilà-Guerau de Arellano et al. (2011) demonstrated that atmospheric dynamics are as crucial as chemistry in interpreting diurnal variations in atmospheric reactants. However, the role of the FT-PBL exchange in HCHO remains underexplored, and the relative importance of vertical exchange on diurnal variations in HCHO compared to that of primary emissions and secondary production remains unclear. Gil et al. (2021, 2023) highlighted the importance of HONO in photochemical oxidation in the Seoul Metropolitan Area, where HONO is formed by the heterogeneous reaction of NO_2 on the aerosol surface constrained by relative humidity.

This study focused on the factors governing the diurnal variation in HCHO:FT-PBL exchange, photochemistry, VOC precursors and primary emissions, heterogeneous HONO production, and dry deposition. Numerical experiments were designed to quantify the role of these factors in determining the diurnal variability in HCHO. Particularly, the relative importance of HCHO and its precursor emissions guides the development of emission control strategies for managing HCHO levels. A zero-order mixed-layer model was employed to simulate PBL dynamics and their interaction with chemistry in a straightforward and computationally efficient manner. Surface emissions and entrainment from the FT were incorporated, which is similar to those of a regional chemical transport model, thereby guiding improvements in the key processes within such models. Finally, the contributions of primary and secondary HCHO to HCHO were assessed using the brute-force method of the first-order approximation and compared with those derived from statistical analyses using chemical tracers.

2. Numerical experiment

2.1. Observations

The Satellite Integrated Joint Monitoring of Air Quality (SIJAQ) 2021 focused on measuring the chemical species of ozone and particulate matter (PM), their gaseous precursors, and the secondary by-products of the photochemical oxidation of the precursors. This study aimed to investigate winter haze formation in Seoul, which took place from October 18 to November 25, 2021, at Olympic Park (OP) and Korea University (KU) in Seoul (Fig. 1). Korea University campus (37.59°N, 127.03°E, 72 m asl.) is located northeast of Seoul, whereas Olympic Park (37.57°E, 127.14°N) is located southeast of Seoul. These two sites were expected to encompass the variability of atmospheric reactants in Seoul. Details of these sites were described by Crawford et al. (2021) and Gil et al. (2023).

At Olympic Park, HCHO was quantitatively analyzed using 2,4-dinitrophenylhydrazine (DNPH) adsorption tubes for automatic semi-real-time adsorption. Briefly, samples were continuously collected at 4-h intervals, resulting in six samples per day. A custom-designed automatic sampler collected atmospheric HCHO every 4 h, forming and adsorbing HCHO-2,4-DNPH derivatives. For extraction, 12 mL of acetonitrile was passed through the DNPH cartridge to elute the samples, which were then diluted 40-fold and analyzed using LC-QTOF. The HCHO-2,4-DNPH derivative introduced into the mass spectrometer was ionized via electrospray ionization and selected at a primary ion mass of 209.0 m/z. Collision energy was then applied to produce secondary mass fragments (45.99, 76.0 m/z) of the DNPH-HCHO complex, which was detected and quantified using TOF with a mass of 45.99 m/z as the final analysis. To ensure the reliability of the analytical results, a minimum of 10 % of the total samples were reanalyzed, and 15 % of the standard samples were tested to maintain accuracy and precision within 5 %. The detailed analytical methods, quality assurance, and quality control can be found in an earlier study (Choe et al., 2022).

At the NIER Seoul supersite near Korea University, the AL4021 HCHO analyzer was used to measure real-time HCHO levels using the Hanch reaction with a time resolution of 10 s. Manual calibration was performed weekly using a standard HCHO source.

NO_x was monitored hourly via photolysis-chemiluminescence, and VOC data were obtained from Photochemical Assessment Monitoring Station (PAMS) sites in Seoul for 54 VOCs (C2–C10) with ozone production potential. The Jongro and Gwangjin PAMS sites, which are closest to Korea University and Olympic Park, respectively, were selected. Additionally, aircraft measurements were employed to determine the relationship of NO_x, O_3, and VOCs between the PBL and FT. The Hanseo Kingair 1900D flowed over Seoul and the West Sea while being equipped with a NO_x monitor and rapid CO analyzer (Park et al., 2020). Chemical sonde measurements were conducted to obtain detailed vertical profiles of ozone from the surface to the lower stratosphere. Sondes for ozone were launched twice daily at Youngin, 40 km south of Olympic Park site (Ryu et al., 2022).

The total vertical amounts of HCHO from the Geostationary Environment Monitoring Spectrometer (Kwon et al., 2019; Kim et al., 2020;

Lee et al., 2024) and the Pandonia Global Network (Herman et al., 2018; Cede et al., 2021) were used to evaluate the simulated vertical profile of HCHO concentration. For comparison, the GEMS pixels covering Seoul were averaged, and two Pandora sites were used to represent the northern and southern parts of Seoul: P54 (37.5644°, 126.9340°) and P149 (37.4580°, 126.9510°). The operational GEMS L2 (version 2) product (https://nesc.nier.go.kr) and PGN L2 data (https://pandonia-global-network.org) were used.

Hourly meteorological data were obtained from the Automated Synoptic Observation System (ASOS) Seoul site of the Korea Meteorological Administration (https://climate.go.kr). PBL heights from the Micro Pulse LIDAR, situated at Seoul National University, and a ceilometer located at Yonsei University, near Korea University, were used for comparison with the modeled PBL heights.

2.2. Numerical model

We employed a mixed layer of MXLCH (Vilà-Guerau de Arellano et al., 2011) for numerical experiments; the computer code is available at https://github.com/classmodel/mxlch. MXLCH is a type of multi-box model allowing for exchanges between the PBL and FT not handled in one-box models. MXLCH vertically stacks three boxes: a mixed layer, a lower FT, and an in-between inversion layer. The mixed layer grows and exchanges heat, moisture, and chemical species with the FT across the inversion layer. When heat, moisture, or chemical species are introduced by surface sources or entrained from the FT, they instantaneously mix within the PBL, similar to that of the one-box model. The vertical structure of the MXLCHx is shown in Fig. 1, which benchmarks the graphical concept proposed by Liu et al. (2021). In winter, mixed layer growth is not strong enough to reach the FT; therefore, many pollutants can be stored in the residual layer at night and transported to the PBL the following morning. MXLCH couples three models: a PBL model (Janssen and Pozzer, 2015), an atmospheric chemical model (Vilà-Guerau de Arellano et al., 2011), and land surface model (van Heerwaarden et al., 2009). PBL dynamics are formulated based on mixed layer theory, which states that atmospheric variables are constant at heights within the PBL due to active mixing. Under a convective boundary layer, chemical species are instantaneously mixed across the PBL as they are emitted, chemically produced, or entrained from FT air. In MXLCH, the inversion layer exhibits an infinitely sharp gradient, which is parameterized as an infinitesimally thin layer, i.e., the jump between the PBL and FT. The PBL growth is explained by the temperature jump shift caused by entrainment from the FT air induced by buoyancy-driven turbulent motion. MXLCH treats PBL dynamics, where the PBL grows as the entrainment induced by the surface buoyancy flux pushes up the inversion layer. Land surface processes, such as surface heat and moisture availability, are predicted by a land surface model representing temporal changes in the ground and surface layer (assumed to be one-tenth of the PBL height) heat/moisture.

We incorporated a simple Nocturnal Boundary Layer (NBL) mechanism into the MXLCH, in which the NBL is stable because radiative cooling decreases with height (hereafter called MXLCHx). The rate equation for the NBL growth follows that of Deardorff (1971) and Yu (1978). Since Deardorff (1971) predicted the NBL height rather than diagnosing it, convective BL (CBL) smoothly transitioned to NBL in the framework of MXLCHx. The transition between the CBL and NBL was determined by the Monin-Obukhov length. It was assumed that the vertical profiles of the heat/moisture/chemical species were uniform within the PBL throughout the day, similar to those of the box model.

We added a carbon bond mechanism (CBM) to MXLCH to represent the detailed features of the NO_x-VOCs-O_3-HO_x system. The CBM lump VOCs via carbon bonds and VOCs with the same bonding type were treated as groups. CB6, the latest version of CBM, was used in this study; it is one of the most widely used mechanisms and is well validated. The emission data currently used to constrain the model do not cover all chemical species, and the VOC observations were primarily focused on PAMS species for which CB6 was particularly well-suited. CB6 comprises 234 chemical reactions and 105 chemical species. The rate coefficients for the chemical reactions were obtained from the CAMx manual (https://camx.com/Files/CAMxUsersGuide_v7.10.pdf) and the photolysis rates by actinic flux were fitted to the observations using the solar zenith angle at 600 MSL/AGL (see Table C-2 in the CAMx manual). A quadratic or cubic polynomial provides a good fit for photolysis rates varying with the solar zenith angle (approximately 0°–86°). HNO_3, a major sink of NO_2, is likely to accumulate in MXLCH simulations. Thus, we treated HNO_3 to equilibrate with the nitrate in the aerosols through gas/particle partitioning. A thermodynamic model of ISORROPIA (Nenes et al., 1998) was coupled with MXLCHx to partition HNO_3 and

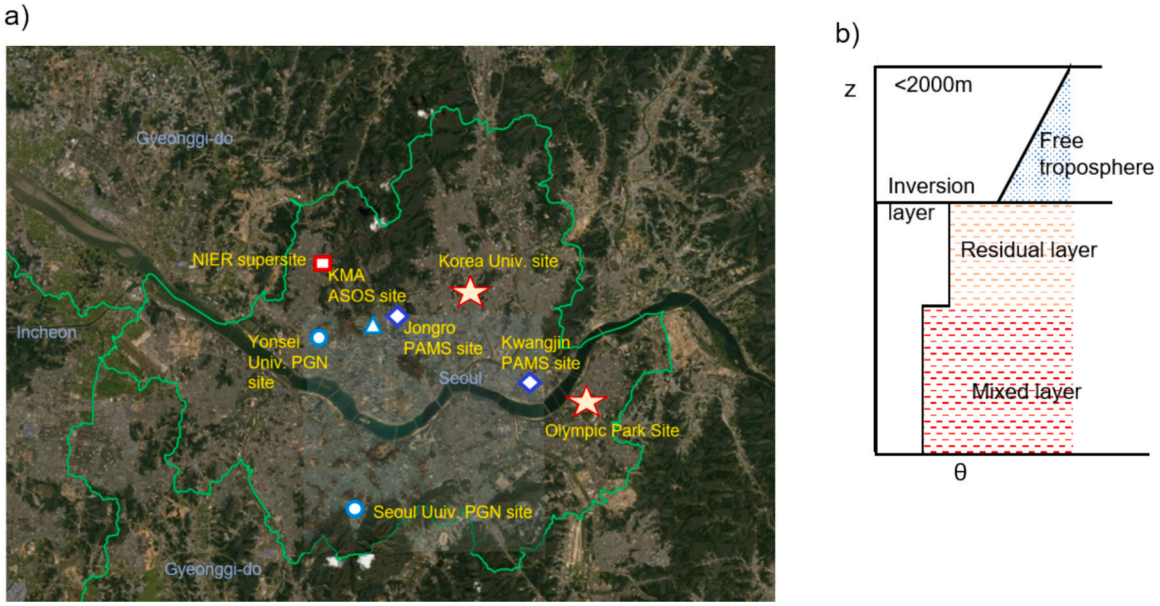

Fig. 1. (a) Map of observation sites during SIJAQ2021 campaign: Korea University and Olympic Park super sites (☆), National Institute of Environmental Research super site (□), KMA ASOS site (△), Yonsei and Seoul University PGN sites (◎), Ministry of Environment PAMS sites (◊), and (b) sketch of vertical structure of MXLCHx for numerical experiments: z represents altitude and θ represents potential temperature.

nitrate.

Dry deposition models utilize multiple resistance analogies to parameterize dry deposition velocity (v_d) on various surfaces (Wesely, 1989). In this study, we adopted a revised parameterization scheme of Zhang et al. (2003) and Wu et al. (2021); the computer code is available at doi: https://doi.org/10.5281/zenodo.4697426 (Zhang and Wu, 2021).

Time-varying surface NOx and VOCs emissions were obtained from the KORUSV5 inventory developed by the Konkuk University for the SIJAQ campaign. KORUS5 uses sparse matrix operator kernel emission (SMOKE-Asia) processing with the input of CAPSS 2021 to split total VOC emissions into CBM6 lumped VOC species with temporal allocations during the campaign period (Woo et al., 2012). The NO_x/VOC emission ratio for Seoul was 1.012021, which was similar to that of the nationwide value of 1.16. SMOKE SECIATE disaggregated VOC emissions into paraffins (34.2 %), xylene (36.1 %), toluene (20.4 %), benzene (13.0 %), terminal olefins + internal olefins (4.7 %), ethylene (1.3 %), HCHO (0.2 %), and other of CBM6 VOC species.

The biogenic isoprene emission rate was estimated using the MEGAN emission factor and a parameterized canopy environment emission activity algorithm (PCEEA) (Guenther et al., 2006). The PCEEA framework was also used to simulate terpene emissions using the methodology outlined by Sakulyanontvittaya et al. (2008) as a reference. In the CB6 chemical mechanism, terpenes are represented as lumped species, with specific compounds, such as α-pinene and sesquiterpenes not explicitly included. To obtain a representative overview, emission factors were derived for typical vegetation types, namely needleleaf and broadleaf trees. Terpene emission factors range from 442 to 869 μg m^{-2} h^{-1}, whereas isoprene emission factors span 2000–12,600 μg m^{-2} h^{-1}. Although terpenes are more reactive than isoprene, their emission rates are 5–10 times lower, resulting in a smaller overall contribution to HCHO concentrations. Leaf area index (LAI) was set in the range of 0–3.51 (m^2 m^{-2}), which is the minimum mean LAI observed in evergreen coniferous and deciduous broadleaf forests in Korea (Lei et al., 2009). When vegetation classification using MODS data (Choi et al., 2010) was applied to Seoul and its surrounding areas, daily average HCHO increased by 11.3 % due to biogenic emissions.

PBL properties are significantly controlled by land surface processes (Deardorff, 1971), such as surface heat and moisture availability. MXLCH adopts the land surface model (van Heerwaarden et al., 2009, 2010, 2011) to simulate temporal changes in the ground and surface layer (assumed to be one-tenth of the PBL height) heat and moisture. This allows for the simultaneous and interactive exchange of energy, water, wind, and chemicals between the surface and the PBL.

A force–restore soil model was employed based on the model formulation of Noilhan and Planton (1989) and the soil temperature formulation from Duynkerke (1991). The soil layer was divided into a thin soil layer above and a deeper soil layer; only the thin soil layer above followed a daily cycle.

Chemical entrainment was used to follow the entrainment of heat and moisture. Thus, the entrainment flux of chemical species depends on the entrainment velocity (PBL growth rate) and the mixing ratio difference (chemical jump) between FT and PBL (Vilà-Guerau de Arellano et al., 2011).

Table 1 lists the initial and boundary conditions (IC/BC) for the control case used in the numerical experiments. SIJAQ-averaged observations were used to prescribe the IC/BC of the meteorological and chemical variables in the MXLCHx. The IC/BC of wind and temperature were obtained from sonde observations twice a day at Osan. Due to the lack of observational data for VOCs in the FT, the IC/BC of VOCs in the FT was inferred from the relationship of CO between the FT and PBL. Vertical CO profiles were obtained using a Hanseo Kingair 1900D aircraft flying over the West Sea during SIJAQ2021. Various instruments aboard the Kingair aircraft collect trace gas and aerosol data (Seo et al., 2019). We set the IC/BC of CO in the FT as one standard deviation from the mean of the Kingair observations (Fig. 2), which corresponds to the 1

Table 1
Initial/boundary concentrations of HCHO and its related chemical species (VOCs precursors and O_3), emission rates of primary HCHO and VOCs precursors, and miscellaneous processes, for numerical experiments.

	HCHO	Olefin	Xylene	Toluene	Ethylene	O_3
Initial and boundary condition in free troposphere (ppb)						
Control	–	0.001	0.001	0.488	0.35	50
Case 1 (a, b)	–	(0.43, 0.5)	(0.53, 1.1)	(2.24, 4.51)	(0.9.1.5)	50
Case 2		0.001	0.001	0.488	0.35	70
Emission rates of primary HCHO and VOCs precursors (μg m^2 s^{-1})						
Control	0.006	0.16	0.89	0.7	0.05	50
Case 3 (a, b)	0.006	0.16 × (0.6, 1.4)	0.89 × (0.6, 1.4)	0.7 × (0.6, 1.4)	0.05 × (0.6, 1.4)	50
Case 4	0.006 × 5	0.16	0.89	0.7	0.05	50
Heterogeneous HONO reaction						
Control	Heterogeneous HONO reaction rate (1.36×10^{-6})					
Case 5	Heterogeneous HONO reaction rate (0)					
Land use category for dry deposition estimation						
Control	Urban					
Case 6	25 USGS land use types					

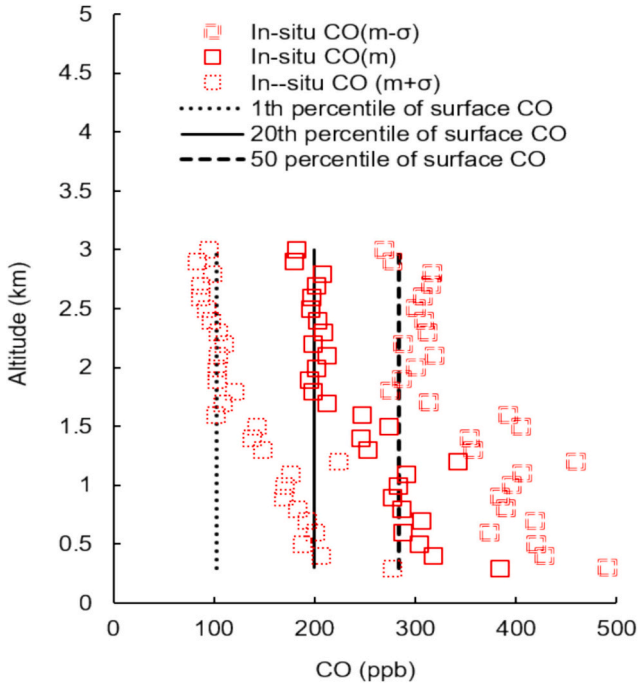

Fig. 2. Comparison of vertical profiles of CO concentrations with uncertainty (±one standard deviation [σ]) from aerial measurements (red box) with 1st, 25th, and 50th percentiles of the observed surface CO concentration at the OP site (black dots).

percentile value of the surface in situ CO observations in Seoul. As with CO, the 1st percentile values of surface in-situ VOCs observations were imposed on the IC/BC of the corresponding VOCs in the FT (see Table 1). The IC/BC of FT NO_2 was set to 1.0 ppb, which was obtained from Kingair 1900D measurements over the West Sea. Ozone sonde measurements in Osan suggested 50 ppb as the IC/BC of FT ozone.

3. Results

3.1. Model evaluation

The meteorological and chemical variations simulated by MXLCHx were evaluated against SIJAQ observations. The SIJAQ-period-averaged concentrations of atmospheric reactants measured at the OP and KU sites were used to evaluate the model performance. The OP and KU sites are spatially located north-south and in downtown and residential areas within Seoul, and are therefore considered representative of the air quality in Seoul.

The SIJAQ was conducted for 39 d from October 18, 2022, to November 25, 2022. Thirty-one-day SIJAQ observations, excluding eight rainy days (daily precipitation (mm) >0 mm), were used for model validation. All chemical species were measured hourly, except for formaldehyde at the OP, which was measured at 4-h intervals. Hourly variations in HCHO levels were obtained using linear interpolation. Fig. 3 shows the time series of air temperature, PBL height, and wind speed between the observations and MXLCHx simulations. MXLCHx reproduced diurnal variations in temperature in the PBL but with a slight time-dependent bias. The observed temperatures were measured at a height of 2 m, whereas the simulated temperatures were the average PBL, resulting in a slight bias towards positive values at night and negative values during the day. This bias did not significantly affect the OH-initiated VOCs oxidation. For example, the rate constant of OH-initiated ethylene oxidation differed by 0.6 % with the maximum temperature difference of 2.2 K at 1300 LT during daytime.

The simulated PBL heights agreed well with those of the LIDAR-derived. Both started to grow around 0700 LT and reached their peaks during 1500–1600 LT, after which they collapsed to approximately 300–400 m by the end of the day. The modeled PBL growth was the result of the entrainment of the FT warmer air into the PBL, which depended on the temperature jump and entrainment flux (assumed to be 0.2 of surface buoyancy flux according to Vilà-Guerau de Arellano et al., 2011) at the PBL top. The simulated decay rates of the PBL were between those obtained from the lidar and ceilometer. The LIDAR- and ceilometer-derived PBL heights were determined from a significant difference in the LIDAR signal due to a sharp decrease in aerosol concentration at the PBL top. As the observed cloud cover averaged 0.2 during SIJAQ period, cloud interference may not have significantly affected PBL evolution during the campaign.

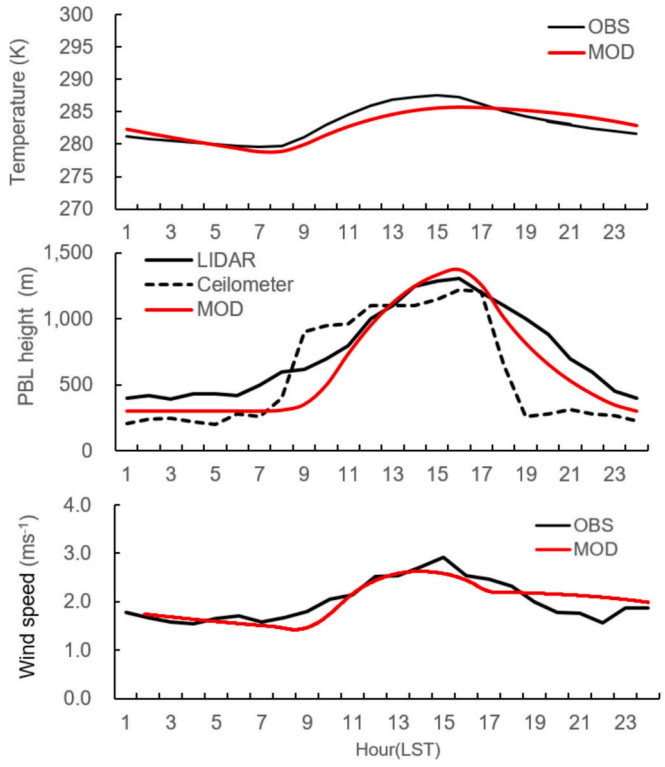

Fig. 3. Diurnal variations of the simulated and observed a) surface temperature, b) PBL height (LIDAR- and Ceilometer-based observations), and c) wind speed during SIJAQ campaign. Black dots and lines indicate observations, whereas red line model simulations.

The hourly mean surface wind speed was in the range of 1.5–2.9 m/s and averaged at 2.0 m/s during the SIJAQ campaign. Light winds create conditions suitable for local emissions to accumulate within the box, thus providing confidence in the steady-state assumptions discussed below. Weather conditions during the SIJAQ campaign were categorized into four synoptic patterns: sustained marine stagnation, transitional stagnant high, continental migratory low, and continental migratory high (Kim et al., 2023). Except for a few days, high-pressure systems were dominant throughout the SIJAQ campaign, which tended to create an environment conducive to air pollution in two ways: atmospheric stagnation and the entrainment of FT pollutants, if present, into the PBL via subsidence.

The model was pre-run until a dynamic equilibrium was reached for the chemical species. At dynamic equilibrium, the concentrations of atmospheric chemicals varied little over time in terms of the daily average. MXLCHx required 3 d to reach dynamic equilibrium, similar to that in the observation-based models employing a master chemical mechanism in a coastal city of southeastern China (Liu et al., 2022). In this study, model chemical species were categorized into two groups. The first group accumulated over time and was constrained by SIJAQ-averaged observations. Pollutant emissions fell into this category and were constrained by the boundary conditions in the PBL and FT obtained from the observations. The second group reached equilibrium between production and losses over time and consisted mainly of secondary pollutants. For example, HCHO reached a quasi-steady state from day 3 in the control run; the diurnal pattern was identical on days 3 and 4, with average daily concentrations differing by <1.0 %. For primary species such as olefins, when constrained, the average daily concentration changed little over time, after day 2, fluctuating by only <0.1 %.

Fig. 4 shows that the model reasonably reproduced the observed diurnal variation in alkanes and alkenes of the VOCs precursors of HCHO. The correlation between the model and the observations was good for propane, ethylene, and olefins (r = 0.7, 0.8, and 0.8, respectively). Propane, a species with a relatively long atmospheric lifetime of approximately 8 weeks during winter (Rosado-Reyes and Francisco, 2007), better reflects the emission characteristics of VOCs.

However, prominent discrepancies were revealed in the diurnal variation of toluene, particularly xylene, between the model simulations and observations. It was reported that m/p-xylene has a temperature dependence comparable to that of isoprene (Kang et al., 2022) cold air can suppress the evaporative emission of xylene during the SIJAQ period. Accordingly, xylene emissions were adjusted by a factor of 0.2 to fit the observations, as shown in Fig. 4c, although the positive bias still remained in the morning hours. The KORUSAQ V5 inventory utilized in this study attributes the majority of toluene and xylene emissions at the two measurement sites to traffic and solvent use. However, the current model failed to accurately represent diurnal variations in emission activities, particularly those associated with solvent use. These discrepancies likely stem from the overestimation of traffic- and solvent-related emissions of the model during morning hours. Future studies should build upon the findings of this study to improve the representation of emissions activities of the model and their temporal variability.

The model revealed prominent discrepancies in the photochemical products (O_3 and HNO_3) and in the demonstrated simulation of O_3, particularly during nocturnal hours (Fig. 4h). In Seoul, a city situated amid mountainous terrain, nocturnal ozone concentrations are markedly influenced by mountain breezes, particularly during spring and autumn seasons (Yun et al., 2024). These breezes facilitate the vertical

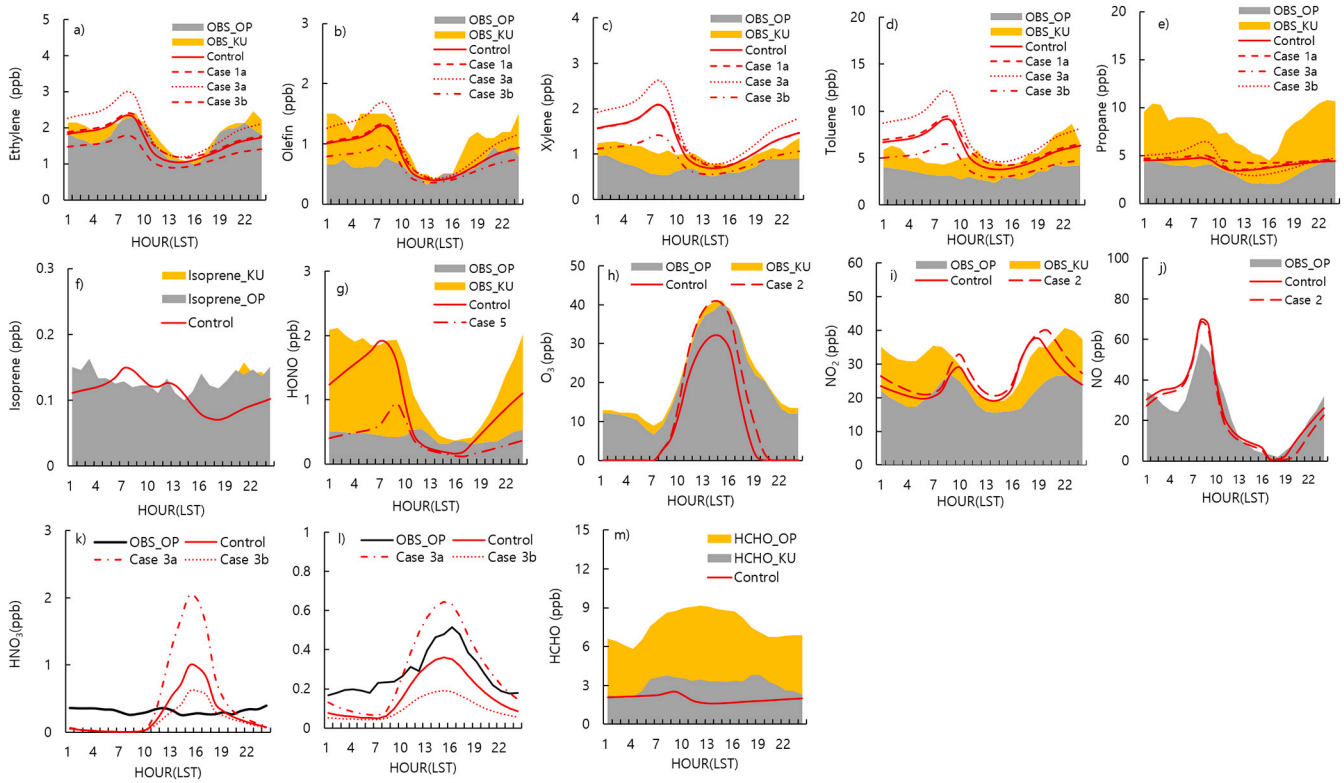

Fig. 4. Diurnal variations of observed and modeled chemical species of a) ethylene, b) olefin, c) xylene, d) toluene, e) propane, f) isoprene, g) HONO, h) O_3, i) NO_2, j) NO, k) peroxyacetyl nitrate (PAN), l) HNO_3, m) HCHO concentrations in Seoul during SIJAQ campaign. VOCs data are from PAMS Kwangjin (OP) and Jongro (KU) sites, and O_3, NO_2, NO, PAN, HNO_3, and HCHO data are from Olympic park (OP) and Korea University (KU) sites averaged during SIJAQ campaign. Case 1 is for FT-PBL exchange, case 2 is for FT O_3 variation, case 3 is for VOCs emission uncertainty, and case 5 is for HONO heterogeneous production.

transport of ozone from the residual layer, contributing to sustained elevated night-time ozone levels. However, this process is not represented in the current model framework, resulting in underestimation of the simulated nighttime ozone concentrations. The measurement of HNO_3 is significantly affected by sampling artifacts. The daytime observations were lower than those of the modeled concentrations due to ground scavenging effects, whereas during the nighttime, the relatively higher indoor temperatures may have facilitated the conversion of aerosol-phase NO_3^- to gaseous HNO_3, potentially maintaining elevated nighttime concentrations. Consequently, it can be inferred that these effects resulted in lower observed concentrations than those of the model during the day and higher concentrations at night.

As shown in Fig. 4m, HCHO concentrations showed poor agreement throughout the day, although the observed HCHO concentrations exhibited significant spatial variability within Seoul. The model underestimated all observations by 1.5–6.9 ppb during daytimes. Furthermore, the model failed to capture the rapid increase in the observed HCHO concentration early in the morning. To validate the vertical profiles of HCHO, the total amount of HCHO was compared from the model against the vertical column densities from GEMS and PGN. The modeled total amount was calculated by integrating HCHO concentrations in PBL and lower FT and background concentrations from OMI observations over Northeast Asia (2.6×10^{15} mol/cm^2) (Baek et al., 2014). The PBL HCHO concentration was integrated from the surface to the top of the PBL, the FT HCHO concentration was integrated from the PBL top to 2 km, and then the background HCHO column density was added to derive the total amount of HCHO.

Fig. 5 shows that both the modeled and observed HCHO amounts increased at similar levels from early morning to afternoon. As in the study by Herman et al. (2018), the model showed a diurnal pattern in which HCHO amounts build up during the day, reached a maximum between 1500 and 1600 LT, and then declined in the evening. Because

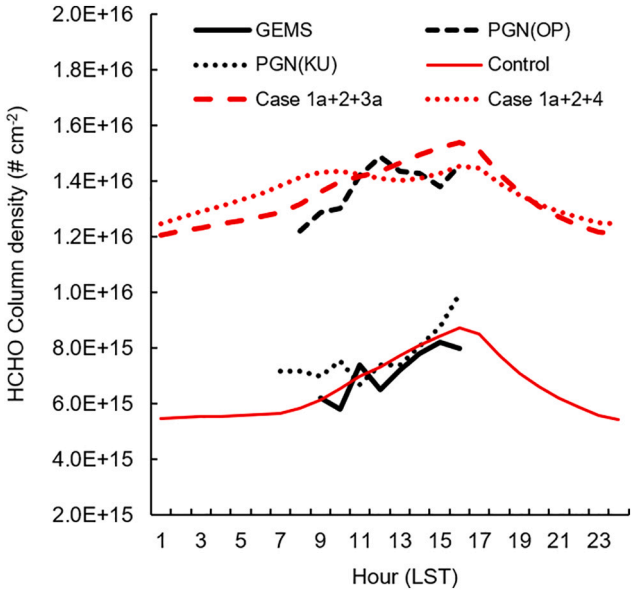

Fig. 5. Comparison of SIJAQ-averaged HCHO total column density (# cm^{-3}) from GEMS, PGN Pandora, and MXLCHx simulations in Seoul. Case 1a + 2 + 3a and case 1a + 2 + 4 are combined cases of higher FT VOC levels (case 1a), higher FT O_3 levels (case 2), and higher VOC emissions (case 3a) and higher HCHO emissions (case 4).

MXLChx reasonably reproduced the temporal evolution of the GEMS HCHO, the uncertainty in turbulent mixing (e.g., PBL growth and exchanges between PBL and FT) may be the potential source of differences between the modeled and observed HCHO. We investigated the role of

relevant physical and chemical processes in determining the causes of the discrepancy between the model and observations.

3.2. Role of controlling factors on HCHO diurnal variation

A numerical experiment was designed to demonstrate the role of the controlling factors in the diurnal evolution of PBL-averaged HCHO: FT-PBL exchange, primary HCHO emission, secondary HCHO production, dry deposition, and heterogeneous HONO production. Here, heterogeneous HONO production was included because of its potential to enhance early morning photochemical activity (Gil et al., 2023). HONO is formed by the heterogeneous catalytic reaction of NO_2 on particles, and when exposed to sunlight in the early morning, OH is released, which influences the subsequent formation of ozone and HCHO. Table 1 summarizes the parameters used in the sensitivity study (i.e., the initial profiles of the meteorological and chemical variables, VOC emission uncertainty, heterogeneous HCHO reaction coefficient, and land-use type). Six cases were designed to cover the sensitivity tests for the five aforementioned factors. The difference between each case and the control case indicates the relative importance of this factor in the diurnal variation in HCHO.

3.2.1. Exchange between FT and PBL

The first numerical experiment investigated the role of the exchange between the FT and PBL in the diurnal variation of HCHO. In Case 1, the initial and boundary conditions of the FT VOC concentrations varied, while keeping the PBL VOCs levels constant (Fig. 2). The FT VOC levels in cases 1a and 1b corresponded to the 25th and 50th percentiles of the VOCs observations at the OP site, respectively. This case was based on a few PTR-TOF-MS measurements aboard Air (1900d), which showed FT VOC levels comparable to those of PBL VOCs during the SIJAQ campaign (not shown here). Fig. 6(a) shows the overall enhancement of HCHO resulting from the entrainment of VOCs rich air during daytime in Case 1; daily mean HCHO increased by up to 119.4 %. Case 1b only increased the simulated HCHO levels between the observed HCHO concentrations at the OP and KU sites. HCHO levels increased in two ways: direct (atmospheric addition) and indirect (OH-initiated VOCs oxidation). Indirect effects originated from an increase in photochemical oxidants (e.g., OH O_3, etc.). For case 1a, the entrainment of higher FT VOCs increased the hydroxyl and methyl peroxy radicals (CH_3O_2) by 25.6 % and 83.8 % at noon, respectively, i.e., OH recycling was promoted by FT-PBL exchange, thereby enhancing HCHO secondary production, mainly from toluene, xylene, ethylene, and olefins. As shown in Fig. 6a, the FT-PBL exchange started at 07:00 LT, entrained high VOCs and HCHO air into the PBL, and stopped at 17:00 LT. The increased HCHO during the daytime was carried over to the next day, resulting in an overall increase in HCHO. The removal processes during the nighttime (e.g., nitrate radical oxidation and dry deposition) had no significant impact on the HCHO levels. Such a relationship of VOCs between the FT and PBL illustrates the importance of the FT-PBL exchange in diurnally varying HCHO.

To distinguish the roles of the entrained FT-VOCs and their accompanying FT-HCHO, we conducted a sensitivity test in which FT-VOCs (FT-HCHO) were set at high (low) values, and vice versa: the 25th percentile of PBL VOCs observations for FT VOCs levels and 1th percentile of PBL-HCHO observations for FT-HCHO levels, and vice versa. The high FT VOCs and low FT HCHO resulted in 38.0 %, 24.3 %, and 89.9 % increases in HCHO, OH, and CH_3O_2, respectively, whereas the high FT HCHO and low FT VOCs resulted in 12.6 %, 3.4 %, and 4.6 % increases in HCHO, OH, and CH_3O_2, respectively. The entrained VOC-rich air promoted OH recycling to enhance HCHO production. Contrarily, the entrained HCHO-rich added HCHO but had little effect on photochemical oxidation: PBL VOCs levels remained unchanged (e.g., $\leq$0.4 % decrease for daily mean olefin and xylene).

3.2.2. Secondary production and primary emissions

Secondary HCHO production relative to primary emissions is important for control and regulatory purposes. Cases 3a and 3b exhibited 40 % higher and lower VOCs precursor emissions, respectively, than those in the control case. This variation is based upon the difference between bottom-up and top-down anthropogenic VOC emissions, which showed that the bottom-up VOCs emissions used in this study differed by a factor of 1.0 $\pm$ 0.4 over Seoul from the top-down VOCs emissions using HCHO column measurements from the Geostationary Trace gas and Aerosol Sensor Optimization spectrometer measurement (Kwon et al., 2021). As shown in Fig. 4, the overall variations in the modeled VOCs concentrations in Case 3 were mainly within the range of the observed VOCs in Seoul, validating the analysis. A 40 % increase (decrease) in VOCs precursor emissions resulted in a 34.4 % (30.0 %) increase (decrease) in the daily mean HCHO. The OH production budget indicated that OH recycling was promoted via the HO_2 + NO reaction. In Case 3a, the main photochemical oxidants, the hydroxyl and peroxyacetyl radicals, increased to a maximum at noon by 37.9 % and 87.0 %%, respectively. Additionally, at 0900 LT, they increased by 27.3 % and 75.4 %, respectively due to the increase in HCHO photolysis. These photochemical oxidants escaped the recycling process as they were oxidized to HNO_3 and PAN (94.4 % and 75.3 % increases in daily average, respectively). The lower-VOCs-emission case showed the opposite result: 30.4 %, 33.5 %, and 53.2 % decreases in HCHO, OH, CH_3O_2, respectively. The overall change in HCHO amounted

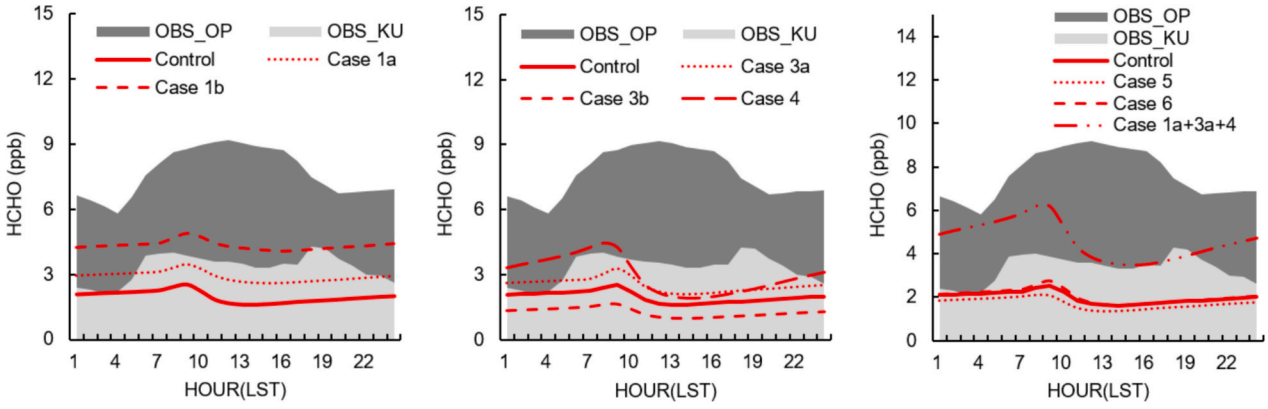

Fig. 6. Comparison of diurnal variations of the observed and simulated average HCHO concentrations during SIJAQ campaign: Olympic Park (OP) in dark gray area and NIER Supersite (KU) in light gray: case 1a (25th percentile of PBL VOCs as FT VOCs), case 1b(50th percentile of PBL VOCs as FT VOCs), case 3a (higher VOCs emission), case 3b (lower VOCs emission), case 4 (higher HCHO emission), case 5 (no HONO heterogeneous production), case 6 (no dry deposition), case 1 + 2 + 3 + 4 (higher FT VOC levels + higher FT O_3 levels + higher VOC emissions + and higher HCHO emissions).

to 64.5 %, although the resulting HCHO concentrations were still below the range of observed HCHO concentrations.

Here, we investigated the impact of primary HCHO emissions on the PBL-averaged HCHO. This case was based on the impact of a cold start on vehicular HCHO emissions. Following Green et al. (2021), Case 4 applied an adjustment factor of 5 to HCHO emissions to consider the increase in emissions due to vehicle cold starts in winter. A five-fold increase in primary HCHO emissions resulted in a 56.8 % increase in daily mean HCHO, although it induced only small changes of 8.5 % and 9.7 % in OH and CH_3O_2, at noon, respectively. This indicates that for primary HCHO, the direct effect is dominant over the indirect effect of additional HCHO production through the enhanced photooxidation of VOCs due to primary HCHO. Although MXLCHx did not allow us to quantify the indirect effect, an earlier study showed that the indirect effect accounted for <10 % of primary HCHO in Mexico City during spring (Volkamer et al., 2010). Because of the increase in primary HCHO, the modeled early morning HCHO fell between the observed morning peaks at the OP and KU sites. Fig. 6 shows that HCHO emissions (case 4) play an important role, comparable to those of the VOCs emissions (case 3a), in the daily variation of HCHO. In earlier studies, the role of primary HCHO varied by day, season, and region, but was found to be significant in the suburbs of Shanghai (Wu et al., 2023) and even higher than that of secondary production in Mexico City (Lei et al., 2009).

3.2.3. Entrainment of free tropospheric ozone

Here, we investigated the impact of ozonolysis on HCHO due to the entrainment of FT O_3. As an oxidant, ozone reacts with alkenes to produce HCHO as a byproduct. Case 2 imposed a higher ozone value of 70 ppb on the IC/BC of FT O_3 while keeping all others the same as that in the control case. This case study was based on ozone sonde measurements during the SIJAQ campaign, showing FT ozone concentrations in the range of 40–70 ppb at altitudes of 1–3 km. The modeled O_3 peak in Case 2 was much closer to that of the observed value than that in the control case (Fig. 6f). Assuming that no FT O_3 was entrained into the PBL, the modeled O_3 concentration was much lower than that of the observed value, i.e., local photochemical production was insufficient to account for the winter ozone in Seoul. Contrary to our expectations, the entrainment of O_3-rich air from the FT into the PBL resulted in a decrease in HCHO levels.

When ozone-rich air was entrained into the atmospheric boundary layer, ozone was photolyzed to produce OH in the presence of H_2O, which reacted with the abundant HCHO present in the PBL, resulting in a decrease in HCHO concentration. Contrastingly, OH induced by O_3 oxidized VOCs to produce HCHO. However, although HCHO had a similar OH reaction rate constant to other VOCs, its concentration was higher than or comparable to that of other VOCs; therefore, the amount of HCHO produced was less than that removed by OH oxidation.

The entrainment of O_3 also induced NOx titration, leading to an increase in oxidized nitrogen compounds; PAN increased by 5.4 % at noon. The production budget for HCHO also showed that the rate of the olefin + O_3 reaction was very low, at 5 % of that of the olefin + OH reaction at noon. Ozonolysis is one of the pathways for VOCs (especially alkene) oxidation but makes a minor contribution to HCHO.

The impact of variations in FT VOCs and O_3 levels, as well as HCHO and VOCs emissions, on ozone formation was examined using the relationship between the ozone mixing ratio and VOCs/NO_2 ratio (Fig. 7). As VOC emissions or FT VOCs increased, the maximum ozone and corresponding VOCs/NO_2 ratio together shifted to higher values. As in Case 2, a higher FT O_3 increased the maximum ozone and shifted the corresponding VOCs/NO_2 ratio to a lower value. However, this shift was not observed in the variations in primary HCHO emissions. It is worth investigating the influence of long-term trend of PBL O_3 on the changes in FT O_3, which showed a long-term increasing trend in Seoul (Lee et al., 2021).

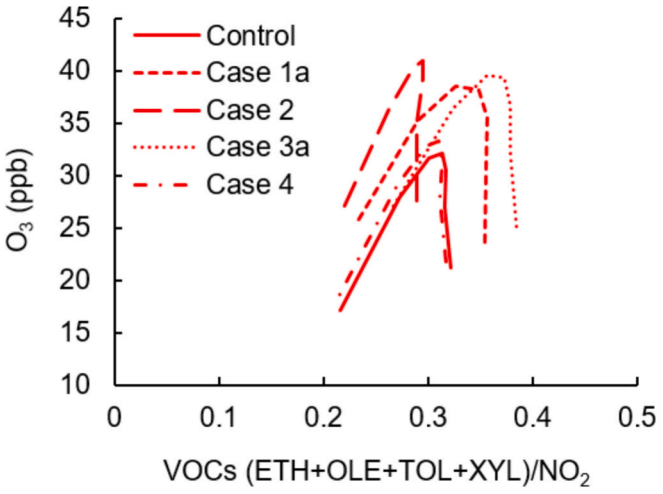

Fig. 7. Comparison of modeled ozone concentration as a function of VOCs (ethylene + olefin + toluene + xylene)/NO_2 ratios for control case with those for Cases 1a (higher FT VOCs), case 2 (higher FT O_3), case 3a (higher VOCs emission), and case 4 (higher HCHO emission).

3.2.4. HONO production and dry deposition

We investigated the role of heterogeneous HONO production by turning the heterogeneous HONO production reaction on and off, as in Case 5. Heterogeneous HONO production resulted in the accumulation of HONO on the particle surface during the night, and when HONO was exposed to sunlight in the morning, it dissociated to release OH, thereby enhancing photochemical reactions (Gil et al., 2021, 2023). Fig. 4 shows that heterogeneous HONO production encompassed the variations in HONO observations in Seoul. As HONO began to photodissociate after sunrise, a HONO peak occurred early in the morning. A 68.1 % increase in HONO at 0700 LT led to a 13.1 % increase in OH at noon, and thus, increased the amount of VOCs oxidation byproducts (e.g., 9.0 % and 15.6 % increase for daily average HCHO and PAN, respectively) and oxidized nitrogen compounds (e.g., 18.9 % increase in daily average HNO_3).

To assess the impact of dry deposition on HCHO, Case 6 varied the land-use types using 25 USGS land-use types. The variations in land use types can lead to the variations in dry deposition velocity (v_d) by up to 8.6 times (e.g., $v_d = 0.3$ cm s^{-1} for urban and $v_d = 2.59$ cm s^{-1} for water-related land use, at noon). The dry deposition velocity in Seoul varied diurnally, being high during the day and low at night. The dry deposition reduced daily average HCHO levels by 8.2 % in Seoul; the effect reached its maximum at 0900 LT.

Therefore, the roles of heterogeneous HONO production and dry deposition are secondary to the roles of FT-PBL exchange and VOC emissions in controlling diurnal HCHO variation.

3.3. Chemical budgets and source contributions

The contributions of different HCHO VOCs precursors were estimated to elucidate the key precursors for HCHO formation. The brute-force Method (BFM) and zero-out were applied to the MXLChx for HCHO budget estimation. The BFM quantifies the sensitivities of the NO_x–VOCs–O_3–HO_x system to VOCs precursors. The brute-force method is a source-sensitivity method for estimating the contribution of a target source to air pollution. Specifically, the zero-out contribution is calculated by perturbing the emissions of the target source to a certain level and performing sensitivity simulations. In this study, the BFM quantified the sensitivity of the NO_x–VOCs–O_3–HO_x system to VOC precursors. Changes in HCHO levels were evaluated by varying the model input of the VOC emissions. The higher the level of emission perturbation, more likely is the occurrence of nonlinear problems and negative

contributions around high-emission sources. However, the lower the level of disturbance, the more likely it is that these can be indistinguishable from inherent model errors. A 20 % emission perturbation was chosen for 10 HCHO model precursors: xylene, toluene, olefin, ethylene, paraffin, acetylene, aldehyde, acetaldehyde, higher aldehyde, and ketone.

First, the modeled HCHO production rates of the lumped model VOC species were evaluated against those of the observed PAMS VOCs species. The former was obtained from 37 chemical reactions in the CBM6 mechanism producing HCHO, whereas the latter was calculated from the reaction with OH for the PAMS VOCs species, as shown in Eq. (1) (Wu et al., 2023).

$$\text{Production rate of HCHO} = \sum_j k_j \gamma_j \,[\text{OH}][\text{VOCs}]_j \quad (1)$$

where k_j and γ_j are reaction rate coefficient and corresponding HCHO yield for the reaction between OH and jth VOCs species, respectively. Over 56 PAMS VOCs species and 24 VOCs species with HCHO yields were used together with the modeled OH concentration to calculate the HCHO production rate. The reaction rate coefficients and corresponding HCHO yields for the reaction with OH were obtained from the literature (Wu et al., 2023) and measured in experiments or field studies during summer in various regions. As shown in Fig. 8a, the modeled and PAMS-based HCHO production rates matched well. The main path from the modeled VOCs to HCHO was CH_3O_2 + NO, followed by olefin + OH and ethylene + OH. CH_3O_2 is an intermediate product of the OH-initiated oxidation of toluene and xylene. The daily mean HCHO production rate from the model was 0.21 ppb h^{-1}, which was a little higher than that of the PAMS VOCs-based rate of 0.14 ppb h^{-1}. This overestimation became evident mid-morning, which may be attributed to the overestimation of toluene and xylene (see Fig. 4). However, the modeled HCHO loss rate originated from two self-photolysis reactions with OH. The observation-based HCHO loss rates were calculated from the observed HCHO concentrations while maintaining the same photolysis frequency and OH concentration as the modeled loss rates. Fig. 8b shows that the modeled HCHO loss rates follow the diurnal pattern of the calculated rates, although at much lower values—0.13 ppb h^{-1} and 0.22 ppb h^{-1} for the modeled and calculated average loss rates, respectively. This was because the modeled HCHO level was much lower than that of the observed HCHO (Fig. 4k).

We investigated the contribution mechanism of the chemical reactions of HCHO to its diurnal variation. Fig. 9 compares the modeled net production rate (Eq. 2) against the observed rates of HCHO concentration change.

$$\text{Net production rate} = \text{chemical production rates} - \text{chemical loss rates} \quad (2)$$

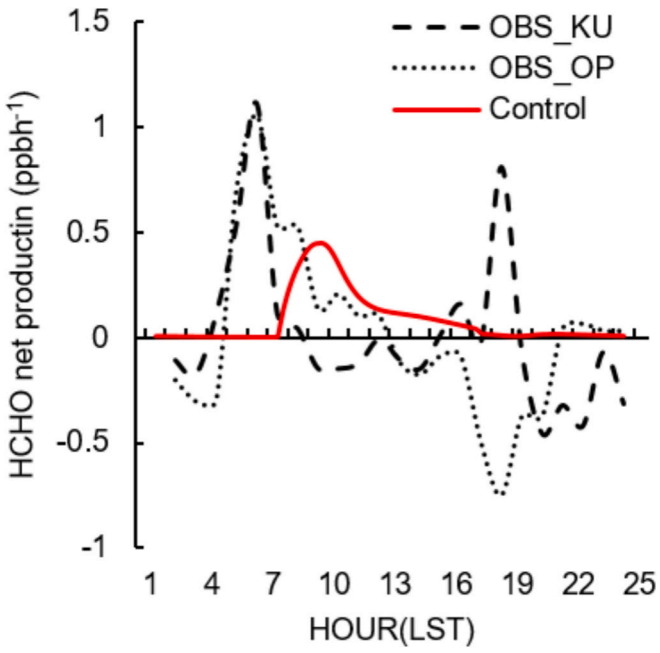

Fig. 9. Average diurnal variations in the calculated net production rates and the observed rates of HCHO concentration change at the Olympic Park (OP) and Korea University (KU) sites during SIJAQ campaign.

The observed rates of HCHO concentration change were much higher than those of the net production during 0500–0800 LT, suggesting that primary emissions caused morning peaks in HCHO at KU and OP. During 0800 LT and 1600 LT, the net production rates were close to those of the observed of HCHO concentration changes at OP, although they were higher than those at KU. At noon, the observed rate of HCHO concentration change was 0.1 ppb h^{-1} in the OP site and the modeled net production rate was similar at 0.13 ppb h^{-1}. This implies that HCHO-poor air from the FT was entrained into the PBL, which significantly diluted HCHO in the KU but only to a small extent in the OP, i.e., the FT HCHO levels can be much higher in the OP downwind of Seoul than those in KU in the city center. The late afternoon peaks in the observed rate of HCHO concentration change at KU were not observed in the modeled net production rate, which seemed to be due to afternoon rush hour traffic at KU.

During daytime (0900–1700 LT), the simulated net production averaged 0.12 ppb h^{-1}, while the observation rate of HCHO concentration change at both OP and KP averaged −0.05 ppb h^{-1}, suggesting

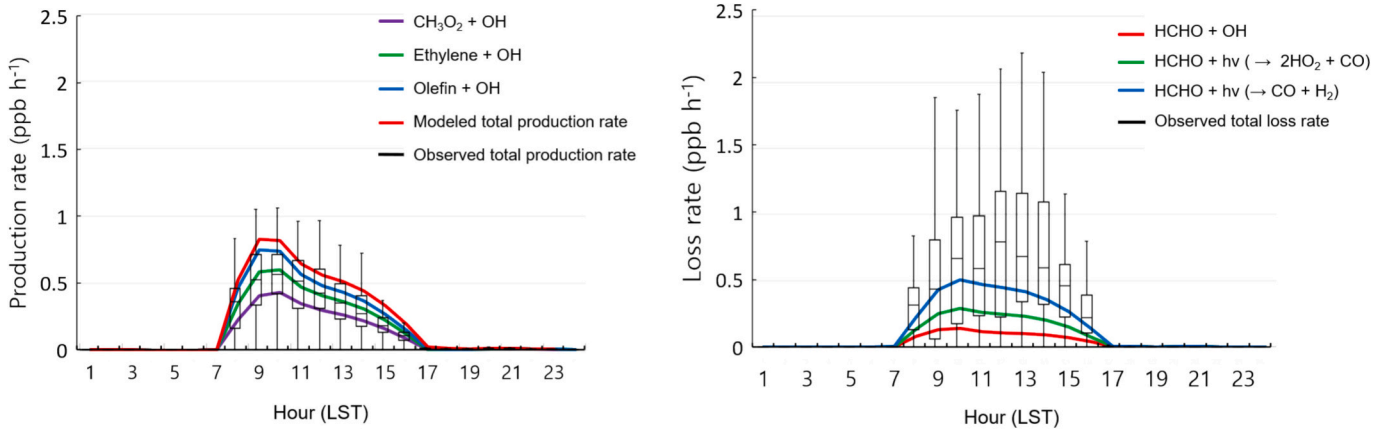

Fig. 8. Diurnal variations in HCHO a) production rate and b) loss rates from the modeled HCHO chemical budget (colored solid lines) and observed VOCs and HCHO concentration (box and whisker plot) during SIJAQ campaign.

that the dilution due to turbulent mixing prevailed chemical net production during daytime in Seoul.

Fig. 10 shows the time series of the percentile contributions of all VOC precursors and primary HCHO emissions to the HCHO concentration. Secondary HCHO production contributed 88.6 % to HCHO, of which olefins (28.8 %), toluene (23.4 %), xylene (15.7 %), ethylene (8.9 %), and biogenic isoprene (11.8 %) were the main contributors. The remaining VOCs, such as paraffin, higher aldehydes, ketones, and acetone, contributed negligibly to the secondary HCHO formation. Aromatics and alkenes had similar influences on HCHO, which is consistent with those of the earlier studies identifying them as major precursors of HCHO (Wang et al., 2017; Wu et al., 2023). According to the 2021 Air Quality Yearbook (https://www.airkorea.or.kr), toluene is the largest contributor to ozone pollution in Seoul, followed by ethylene. During KORUS-AQ (May 25–June 2, 2016), ozone formation in Seoul was the most sensitive to aromatic substances (Simpson et al., 2020). Therefore, managing common sources of aromatic compounds and alkenes is effective for simultaneously mitigating ozone and HCHO pollution. Contrarily, the primary HCHO emissions contributed to 13.7 % of its concentration. Choe et al. (2022) used a linear regression model for HCHO, toluene, and O_x (O_3 + NO_2) observations at the OP site to separate primary and secondary HCHO and suggested that secondary HCHO plays a dominant role over primary HCHO. However, when impact of cold start on HCHO emissions was considered in the control case, the contribution of primary HCHO increased up to 42.0 %, while that of secondary production decreased to 56.1 %. The primary HCHO is as important as secondary production in determining daily HCHO, which is similar to that of earlier studies emphasizing the importance of primary emissions: 38.5 % from primary vehicular emissions and 8.9 % from industrial emissions in Houston-Galveston airshed in September (Rappenglück et al., 2010) and up to 50 % on daily basis in Mexico City in April (Lei et al., 2009).

The contribution of the control factors to HCHO varied at different stages of the PBL evolution; primary HCHO was the main contributor during morning rush hours (0600–0800 LT), whereas secondary HCHO was dominant during the day. Changes in primary and secondary HCHO contributions at different stages of the PBL evolution were also observed in other cities, such as Shanghai (Wu et al., 2023) and Mexico City (Lei et al., 2009).

However, the contribution of dry deposition peaked at 0900 LT due to the highest HCHO concentration. Heterogeneous HONO production also contributed the most at 1000 LT due to OH release from the accumulated HONO during the night.

4. Conclusion

We used an observation-constrained mixed-layer model to identify the key factors controlling the daily variations in HCHO. The model, which is capable of simultaneously handling chemical and meteorological processes in the PBL, demonstrated its usefulness in numerical experiments. Therefore, we investigated the roles of FT–PBL exchange, primary and secondary HCHO production, heterogeneous HONO production, and dry deposition on the diurnal variation of HCHO in Seoul. Large variations in HCHO resulted from uncertainties in VOCs and HCHO emissions and the FT–PBL exchange. More reliable information on VOCs and HCHO emission inventories and FT VOCs is required to interpret the daily varying HCHO levels in the PBL.

During the SIJAQ campaign period, secondary HCHO production dominated primary HCHO emissions in Seoul, which is similar to that of the results of a tracer-based statistical approach for southeastern Seoul (Choe et al., 2022). However, when considering the impact of a cold climate on vehicular HCHO emissions, the proportion of primary HCHO increased to a level similar to that of secondary HCHO emissions. Aromatics (toluene and xylene) and alkenes (olefins and ethylene) made similar contributions to HCHO, which is similar to those of many earlier studies indicating both of these as major sources of secondary HCHO. The strong correlation between VOC emissions (aromatics and alkenes) and photochemical products (HCHO and O_3) suggests that emission regulations for common VOC emissions are effective in mitigating HCHO and O_3 pollution in Seoul.

As the PBL evolves throughout the day, the importance of the control elements changes accordingly. Primary HCHO, heterogeneous HONO production, and dry deposition play important roles, mainly in the morning, whereas secondary HCHO and FT–PBL exchange play dominant roles during the day.

The mixed-layer model of MXLCHxs treat physical and chemical processes similar to those of a three-dimensional chemical transport model, indicating its usefulness for interpreting simulation results and improving the chemical transport model.

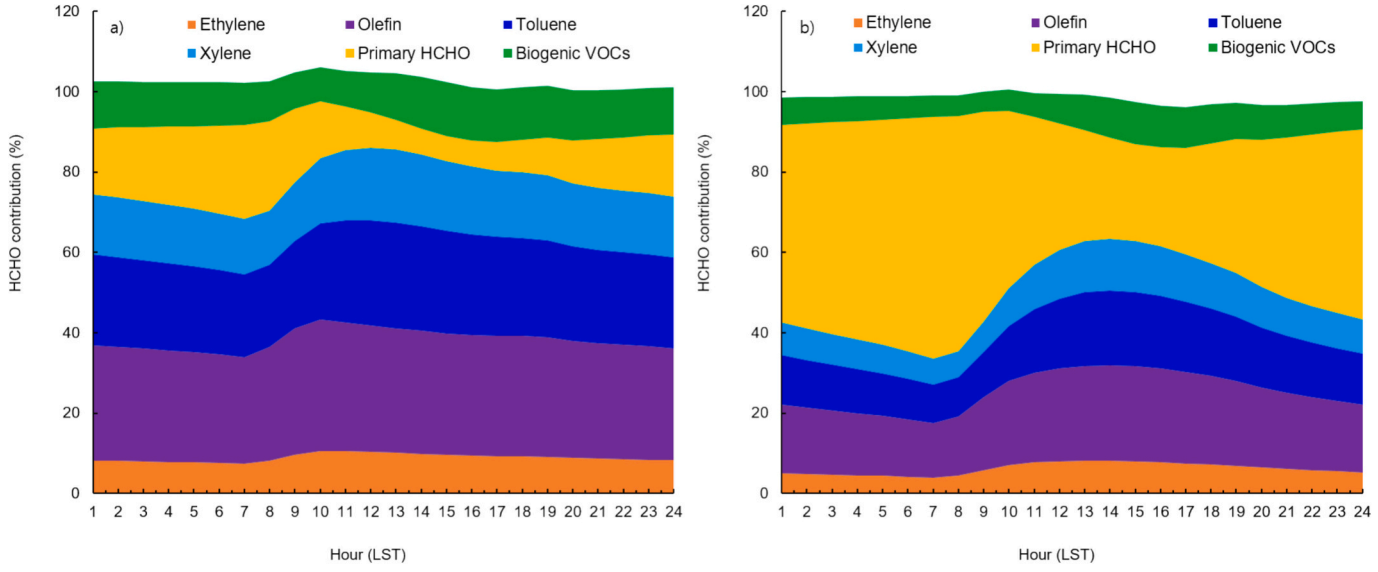

Fig. 10. Relative contribution of VOCs precursor emissions and primary HCHO emissions to HCHO in Seoul during the SIJAQ campaign a) with and b) without cold start HCHO emissions.

CRediT authorship contribution statement

Lim-Seok Chang: Writing – review & editing, Writing – original draft, Visualization, Validation, Software, Methodology, Formal analysis, Conceptualization. **Soi Ahn:** Visualization, Data curation. **Min-Suk Bae:** Investigation. **Seung-Myung Park:** Investigation. **Junsu Gil:** Investigation. **Kwang-Rae Kim:** Investigation. **Gangwoong Lee:** Supervision. **Taehyoung Lee:** Investigation. **Jung-Hun Woo:** Investigation. **Rokjin Park:** Investigation. **Hyeong-Ahn Kwon:** Validation. **Gyo-Hwang Choo:** Investigation. **Chang-Keun Song:** Supervision.

Declaration of competing interest

The authors declare that they have no known competing financial interests or personal relationships that could have appeared to influence the work reported in this paper.

Acknowledgment

We thank Kees van den Dries, Huug Ouwersloot, and Jordi Vilà-Guerau de Arellano for sharing the source code for MXLCH and the PIs of SIJAQ campaign, as well as, support staff for establishing and maintaining the Seoul and Seoul-SNU sites of the PGN used in this investigation. We would like to thank Editage (www.editage.co.kr) for English language editing. This study was supported by grants from the National Institute of Environmental Research (Grant Number NIER-2023-01-01-023) and the Korea Environment Industry & Technology Institute through "Climate change R&D Project for New Climate Regime" funded by the Korea Ministry of Environment (Grant Number 2022003560002).

Data availability

Data will be made available on request.

References

Baek, K.H., Kim, J.H., Park, R.J., Chance, K., Kurosu, T.P., 2014. Validation of OMI HCHO data and its analysis over Asia. Sci. Total Environ. 490, 93–105.

Cede, A., Tiefengraber, M., Gebetsberger, M., Kreuter, M., 2021. TN on manual for Blick software Suite 1.8. Pandonia Global Network. https://www.pandonia-global-network.org/wpcontent/uploads/2021/09/BlickSoftwareSuit_Manual_v1-8-4.pdf.

Choe, S., Oh, S.-H., Kim, M., Song, M.-K., Yu, G.-H., Chang, L.-S., Shin, S.-A., Bae, M.-S., 2022. Effect of secondary HCHO and ozone formation during SIJAQ 2021 campaign — analysis of HCHO-2,4-DNPH using LC/QTOF. J. Korean Soc. Atmos. Environ. 38, 577–587. https://doi.org/10.5572/KOSAE.2022.38.4.577.

Choi, H.-A., Lee, W.-K., Son, Y., Kojima, T., Muraoka, H., 2010. Vegetation classification using seasonal variation MODIS data. Korean J. Remote Sens. 26 (6), 665–673.

Crawford, J.H., Ahn, J.-Y., Al-Saadi, J., Chang, L., Emmons, L.K., Kim, J., Lee, G., Park, J.-H., Park, R.J., Woo, J.H., Song, C.-K., Hong, J.-H., Hong, Y.-D., Lefer, B.L., Lee, M., Lee, T., Kim, S., Min, K.-E., Yum, S.S., Shin, H.J., Kim, Y.-W., Choi, J.-S., Park, J.-S., Szykman, J.J., Long, R.W., Jordan, C.E., Simpson, I.J., Fried, A., Dibb, J. E., Cho, S.Y., Kim, Y.P., 2021. The Korea–United States Air Quality (KORUS-AQ) field study. Elem. Sci. Anthrop. 9 (1). https://doi.org/10.1525/elementa.2020.00163.

Deardorff, J.W., 1971. Rate of growth of the nocturnal boundary layer. Paper presented at Symposium on Air Pollution, Turbulence and Diffusion. Las Cruces, N.M., NCAR ms. No. 71-246.

Dovrou, E., Bates, K.H., Moch, J.M., Mickley, L.J., Jacob, D.J., Keutsch, F.N., 2022. Catalytic role of formaldehyde in particulate matter formation. Proc. Natl. Acad. Sci. U. S. A. 119. https://doi.org/10.1073/pnas.2113265119 e2113265119.

Duynkerke, P.G., 1991. Radiation fog: a comparison of model simulation with detailed observations. Mon. Weather Rev. 119, 324–341.

Garcia, A.R., Volkamer, R., Molina, L.T., Molina, M.J., Samuelson, J., Mellqvist, J., Galle, B., Herndon, S.C., Kolb, C.E., 2006. Separation of emitted and photochemical formaldehyde in Mexico City using a statistical analysis and a new pair of gas-phase tracers. Atmos. Chem. Phys. 6, 4545–4557. https://doi.org/10.5194/acp-6-4545-2006.

Gil, J., Kim, J., Lee, M., Lee, G., An, J., Lee, D.S., Jung, J., Cho, S., Whitehill, A., Szykman, J., Lee, J., 2021. Characteristics of HONO and its impact on O_3 formation in the Seoul Metropolitan Area during the Korea-US Air Quality study. Atmos. Environ. 247, 118182. https://doi.org/10.1016/j.atmosenv.2020.118182.

Gil, J., Lee, M., Lee, H., Jang, J., 2023. Seasonal characteristics of HONO variations in Seoul during 2021–2022. J. Korean Soc. Atmos. Environ. 39, 308–319. https://doi.org/10.5572/KOSAE.2023.39.3.308.

Green, J.R., Fiddler, M.N., Fibiger, D.L., McDuffie, E.E., Aquino, J., Campos, T., Shah, V., Jaeglé, L., Thornton, J.A., DiGangi, J.P., Wolfe, G.M., Bililign, S., Brown, S.S., 2021. Wintertime formaldehyde: airborne observations and source apportionment over the Eastern United States. J. Geophys. Res.-Atmos. 126, e2020JD033518. https://doi.org/10.1029/2020JD033518.

Gupta, K.C., Ulsamer, A.G., Preuss, P.W., 1982. Formaldehyde in indoor air: sources and toxicity. Environ. Int. 8, 1–6.

Herman, J., Spinei, E., Fried, A., Kim, J., Kim, J., Kim, W., Cede, A., Abuhassan, N., Segal-Rozenhaimer, M., 2018. NO_2 and HCHO measurements in Korea from 2012 to 2016 from Pandora spectrometer instruments compared with OMI retrievals and with aircraft measurements during the KORUS-AQ campaign. Atmos. Meas. Tech. 11, 4583–4603. https://doi.org/10.5194/amt-11-4583-2018.

IARC, 2006. Formaldehyde, 2-Butoxyethanol and 1-Tert-Butoxypropan-2-Ol. In: International Agency for Research on Cancer. In: IARC Monographs on the Evaluation of Carcinogenic Risks to Humans. IARC, Lyon.

Janssen, R.H.H., Pozzer, A., 2015. Description and implementation of a MiXed Layer model (MXL, v1.0) for the dynamics of the atmospheric boundary layer in the Modular Earth Submodel System (MESSy). Geosci. Model Dev. 8, 453–471. https://doi.org/10.5194/gmd-8-453-2015.

Kang, S., Kim, J.-A., Lee, M., Park, J., Jeon, E., Shim, M., Shin, Y., 2022. An analysis of the temporal variability in volatile organic compounds (VOCs) within megacity Seoul and and identification of their sources. Atmos. Pollut. Res. 13, 101338.

Kim, C.-H., Jo, H.-Y., Jo, Y.-J., Lee, H.-J., Kim, J.-M., Lee, N.-M., Jeong, S.-Y., Baek, S.-H., Park, M.-J., Chang, L.-S., Lee, J.-J., Song, C.-K., 2023. Synoptic meteorological conditions and contributing factors to air quality during the SIJAQ campaign. Atmos. Environ. 309. https://doi.org/10.1016/j.atmosenv.2023.119939.

Kim, J., Jeong, U., Ahn, M.H., Kim, J.H., Park, R.J., Lee, H., Song, C.H., Choi, Y.S., Lee, K. H., Yoo, J.M., Jeong, M.J., Park, S.K., Lee, K.M., Song, C.K., Kim, S.W., Kim, Y.J., Kim, S.W., Kim, M., Go, S., Liu, X., Chance, K., Chan Miller, C., Al-Saadi, J., Veihelmann, B., Bhartia, P.K., Torres, O., Abad, G.G., Haffner, D.P., Ko, D.H., Lee, S. H., Woo, J.H., Chong, H., Park, S.S., Nicks, D., Choi, W.J., Moon, K.J., Cho, A., Yoon, J., Kim, S., Hong, H., Lee, K., Lee, H., Lee, S., Choi, M., Veefkind, P., Levelt, P. F., Edwards, D.P., Kang, M., Eo, M., Bak, J., Baek, K., Kwon, H.A., Yang, J., Park, J., Han, K.M., Kim, B.R., Shin, H.W., Choi, H., Lee, E., Chong, J., Cha, Y., Koo, J.H., Irie, H., Hayashida, S., Kasai, Y., Kanaya, Y., Liu, C., Lin, J., Crawford, J.H., Carmichael, G.R., Newchurch, M.J., Lefer, B.L., Herman, J.R., Swap, R.J., Lau, A.K. H., Kurosu, T.P., Jaross, G., Ahlers, B., Dobber, M., McElroy, C.T., Choi, Y., 2020. New era of air quality monitoring from space: geostationary environment monitoring spectrometer (GEMS). Bull. Am. Meteorol. Soc. 101, E1–E22. https://doi.org/10.1175/BAMS-D-18-0013.1.

Kwon, H.-A., Park, R.J., González Abad, G., Chance, K., Kurosu, T.P., Kim, J., De Smedt, I., Van Roozendael, M., Peters, E., Burrows, J., 2019. Description of a formaldehyde retrieval algorithm for the Geostationary Environment Monitoring Spectrometer (GEMS). Atmos. Meas. Tech. 12, 3551–3571. https://doi.org/10.5194/amt-12-3551-2019.

Kwon, H.-A., Park, R.J., Oak, Y.J., Nowlan, C.R., Janz, S.J., Kowalewski, M.G., Fried, A., Walega, J., Bates, K.H., Choi, J., Blake, D.R., Wisthaler, A., Woo, J.-H., 2021. Top-down estimates of anthropogenic VOCs emissions in South Korea using formaldehyde vertical column densities from aircraft during the KORUS-AQ campaign. Elem. Sci. Anthrop. 9. https://doi.org/10.1525/elementa.2021.00109.

Lee, G.T., Park, R.J., Kwon, H.-A., Ha, E.S., Lee, S.D., Shin, S., Ahn, M.-H., Kang, M., Choi, Y.-S., Kim, G., Lee, D.-W., Kim, D.-R., Hong, H., Langerock, B., Vigouroux, C., Lerot, C., Hendrick, F., Pinardi, G., De Smedt, I., Van Roozendael, M., Wang, P., Chong, H., Cho, Y., Kim, J., 2024. First evaluation of the GEMS formaldehyde product against TROPOMI and ground-based column measurements during the in-orbit test period. Atmos. Chem. Phys. 24, 4733–4749. https://doi.org/10.5194/acp-24-4733-2024.

Lee, H.-J., Chang, L.-S., Jaffe, D.A., Bak, J., Liu, X., Abad, G.G., Jo, H.-Y., Jo, Y.-J., Lee, J.-B., Kim, C.-H., 2021. Ozone continues to increase in East Asia despite decreasing NO_2: causes and abatements. Remote Sens. (Basel) 13, 2177. https://doi.org/10.3390/rs13112177.

Lei, W., Zavala, M., de Foy, B., Volkamer, R., Molina, M.J., Molina, L.T., 2009. Impact of primary formaldehyde on air pollution in the Mexico City Metropolitan Area. Atmos. Chem. Phys. 9, 2607–2618. https://doi.org/10.5194/acp-9-2607-2009.

Liu, Y., Tang, G., Wang, M., Liu, B., Hu, B., Chen, Q., Wang, Y., 2021. Impact of residual layer transport on air pollution in Beijing, China. Environ. Pollut. 271, 116325. https://doi.org/10.1016/j.envpol.2020.116325.

Liu, T., Li, M., Xu, L, Chen, J., Bian, Y., Yang, C., Dan, Y., Zhang, Y., Xue, L., Zhao, M., Huang, Z., Wang, H., 2022. Atmospheric oxidation capacity and ozone pollution mechanism in a coastal city of southeastern China: analysis of a typical photochemical episode by an observation-based model. Atmos. Chem. Phys. 22, 2173–2190. https://doi.org/10.5194/acp-22-2173-2022.

Nenes, A., Pandis, S.N., Pilinis, C., 1998. ISORROPIA: a new thermodynamic equilibrium model for multiphase multicomponent inorganic aerosols. Aquat. Geochem. 4, 123–152. https://doi.org/10.1023/A:1009604003981.

Noilhan, J., Planton, S., 1989. A simple parameterization of land surface processes for meteorological models. Mon. Weather Rev. 117, 536–549.

Park, T., Choi, Y., Choi, J., Ahn, J., Park, J., Lee, Y., Ban, J., Park, G., Kang, S., Kim, K., 2020. Aircraft measurements of physicochemical evolution of atmospheric aerosols in air pollution plumes over a megacity and suburban areas. Aerosol Air Qual. Res. 20, 2485–2494. https://doi.org/10.4209/aaqr.2019.12.064920.

Possanzini, M., Palo, V.D., Cecinato, A., 2002. Sources and photodecomposition of formaldehyde and acetaldehyde in Rome ambient air. Atmos. Environ. 36, 3195–3201. https://doi.org/10.1016/S1352-2310(02)00192-9.

Rappenglűck, B., Dasgupta, P.K., Leuchner, M., Li, Q., Luke, W., 2010. Formaldehyde and its relation to CO, PAN, and SO_2 in the Houston-Galveston airshed. Atmos. Chem. Phys. 10, 2413–2424. https://doi.org/10.5194/acp-10-2413-2010.

Rosado-Reyes, C.M., Francisco, J.S., 2007. Atmospheric oxidation pathways of propane and its by-products: Acetone, acetaldehyde, and propionaldehyde. J. Geophys. Res.-Atmos. 112, D14310. https://doi.org/10.1029/2006JD007566.

Ryu, H., Koo, J.-H., Kim, J.-G., Lee, N., Lee, W.-J., Kim, J., 2022. The observation of ozone vertical profile in Yongin, Korea during the GMAP 2021 field campaign. Atmosphere. https://doi.org/10.14191/Atmos.2022.32.3.247.

Sakulyanontvittaya, T., Duhl, T., Wiedinmyer, C., Helmig, D., Matsunaga, S., Potosnak, M., Milford, J., Guenther, A., 2008. Monoterpene and sesquiterpene emissions estimates for the United Sates. Environ. Sci. Technol. 42, 1623–1629.

Seo, B.-K., Park, S.b., Lee, D., Yu, M., Yu, J., Bae, K.-N., Ahn, J., Park, J., Kim, S., Lee, T., Kim, J., 2019. Airborne Inlets and Instrumentation on Aircraft Platform for Air Quality Observation. J. Korean Soc. Atmos. Environ. 35, 815–830.

Simpson, I.J., Blake, D.R., Blake, N.J., Meinardi, S., Barletta, B., Hughes, S.C., Fleming, L. T., Crawford, J.H., Diskin, G.S., Emmons, L.K., Fried, A., Guo, H., Peterson, D.A., Wisthaler, A., Woo, J.-H., Barré, J., Gaubert, B., Kim, J., Kim, M.J., Kim, Y., Knote, C., Mikoviny, T., Pusede, S.E., Schroeder, J.R., Wang, Y., Wennberg, P.O., Zeng, L., 2020. Characterization, sources and reactivity of volatile organic compounds (VOCs) in Seoul and surrounding regions during KORUS-AQ. Elem. Sci. Anthrop. 8. https://doi.org/10.1525/elementa.434.

van Heerwaarden, C.C., Vilà-Guerau de Arellano, J., Moene, A.F., Holtslag, A.A.M., 2009. Interactions between dry-air entrainment, surface evaporation and convective boundary layer development. Q. J. Roy. Meteorol. Soc. 135, 1277–1291. https://doi.org/10.1002/qj.431.

van Heerwaarden, C.C., Vilà-Guerau de Arellano, J., Gounou, A., Guichard, F., Couvreux, F., 2010. Understanding the daily cycle of evaportranspiration: a method to quantify the influence of forcings and feedbacks. J. Hydrometeorol. 11, 1405–1422.

van Heerwaarden, C.C., 2011. Surface Evaporation and Water Vapor Transport in the Convective Boundary Layer. PhD thesis. Wageningen University, Wageningen, the Netherlands.

Vilà-Guerau de Arellano, J., Patton, E.G., Karl, T., van den Dries, K., Barth, M.C., Orlando, J.J., 2011. The role of boundary layer dynamics on the diurnal evolution of isoprene and the hydroxyl radical over tropical forests. J. Geophys. Res. 116, D07304. https://doi.org/10.1029/2010JD014857.

Volkamer, R., Sheehy, P., Molina, L.T., Molina, M.J., 2010. Oxidative capacity of the Mexico City atmosphere — part 1: a radical source perspective. Atmos. Chem. Phys. 10, 6969–6991. https://doi.org/10.5194/acp-10-6969-2010.

Vrekoussis, M., Wittrock, F., Richter, A., Burrows, J.P., 2010. GOME-2 observations of oxygenated VOCs: what can we learn from the ratio of glyoxal to formaldehyde on a global scale? Atmos. Chem. Phys. 10, 10145–10160. https://doi.org/10.5194/acp-10-10145-2010.

Wang, C., Huang, X.-F., Han, Y., Zhu, B., He, L.-Y., 2017. Sources and potential photochemical roles of formaldehyde in an urban atmosphere in South China. J. Geophys. Res.-Atmos. 122. https://doi.org/10.1002/2017JD027266.

Wesely, M.L., 1989. Parameterization of surface resistances to gaseous dry deposition in regional-scale numerical models. Atmos. Environ. 23, 1293–1304.

Woo, J.-H., Choi, K.-C., Kim, H.K., Baek, B.H., Jang, M., Eum, J.-H., Song, C.H., Ma, Y.-I., Sunwoo, Y., Chang, L.-S., Yoo, S.H., 2012. Development of an anthropogenic emissions processing system for Asia using SMOKE. Atmos. Environ. 58, 5–13. https://doi.org/10.1016/j.atmosenv.2011.10.042.

Wu, Y., Huo, J., Yang, G., Wang, Y., Wang, L., Wu, S., Yao, L., Fu, Q., Wang, L., 2023. Measurement report: production and loss of atmospheric formaldehyde at a suburban site of Shanghai in summertime. Atmos. Chem. Phys. 23, 2997–3014. https://doi.org/10.5194/acp-23-2997-2023.

Wu, Z., Zhang, L., Walker, J.T., Makar, P.A., Perlinger, J.A., Wang, X., 2021. Extension of a gaseous dry deposition algorithm to oxidized volatile organic compounds and hydrogen cyanide for application in chemistry transport models. Geosci. Model Dev. 14, 5093–5105. https://doi.org/10.5194/gmd-14-5093-2021.

Yu, T.-W., 1978. Determining height of the nocturnal boundary layer. J. Appl. Meteorol. 17, 28–33. https://doi.org/10.1175/1520-0450(1978)017<0028:DHOTNB>2.0.CO;2.

Yun, C., Kim, J., Lee, J., Lee, J., Gil, J., Lee, M., Lee, G., 2024. Nocturnal downward transport of NO_3 radical from the residual layer to a surface site by the mountain breeze in Seoul, South Korea. Atmos. Environ. 321. https://doi.org/10.1016/j.atmosenv.2024.120345.

Zhang, L, Wu, Z., 2021. A computer code for calcuating dry deposition velocities for 45 gaseous species. https://zenodo.org/records/4697426.

Zhang, L., Brook, J.R., Vet, R., 2003. A revised parameterization for gaseous dry deposition in air-quality models. Atmos. Chem. Phys. 3, 2067–2082. https://doi.org/10.5194/acp-3-2067-2003.